Journal of Materials Chemistry C

Accepted Manuscript

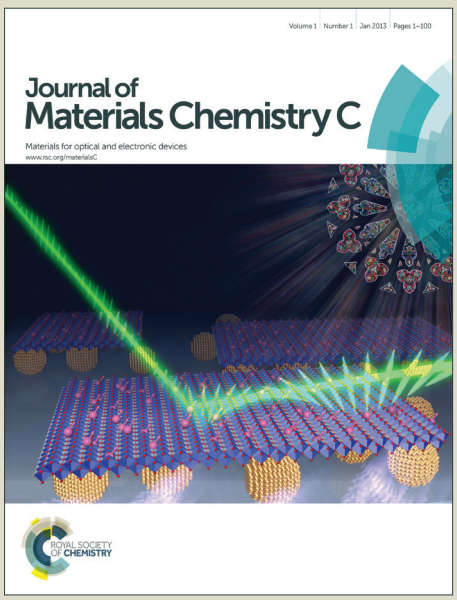

ROYAL SOCIETY OF CHEMISTRY

www.rsc.org/materialsC

Cite this: DOI: 10.1039/c0xx00000x

www.rsc.org/xxxxxx

ARTICLE TYPE

Structure Transition and Magnetism of BCC Ni Nanowires

C. Han,*[a] K. G. Chang,[a] S. Yang,[a] P. P Wang,[a,b] Ri-ichi Murakami,[b] and X. P. Song *[a]

Received (in XXX, XXX) Xth XXXXXXXXX 20XX, Accepted Xth XXXXXXXXX 20XX
DOI: 10.1039/b000000x

Body-Centered-Cubic (BCC) Ni nanowires have been successfully synthesized by a multistep ac electro-deposition in anodic aluminium oxide templates. Bcc Ni is ferromagnetic with a lattice constant of 0.288 nm, and bcc-Ni to fcc-Ni phase transition occurs in heat treatment. Magnetic measurements suggest that the ferromagnetic transition of bcc Ni nanowires involves a structure change evolving from bcc to fcc in magnetic-ordering process. Furthermore, the processes of structure transition in bcc Ni nanowires under the heating conditions are observed in situ by transmission electron microscopy. In addition, our work also establishes that fcc Ni nanowires and bulk Ni have only a ferromagnetic transition in the curie point, respectively, involving no crystal structure change.

Introduction

Ferromagnetic nanowires have been widely investigated in the last decade. Besides foundational researches[1-3], ferromagnetic nanowires have also been made the potential applications in magnetic and electronic nanodevices[4-7]. As the traditional-ferromagnetic transition metals, Nickel has been intensively studied for ferromagnetic properties of the powders, films, and nanowires[8-15].

It is known that face-centered-cubic (fcc) Nickel structure is a better stability in bulk, but hexagonal closed-packed (hcp) and body-centered-cubic (bcc) Nickel structure is meta-stable in bulk and does not exist naturally, respectively. However, as the grain size of these metals goes small into nano-scale, with an increasing ratio of surface atoms, their structures and magnetic properties make a sudden change in some critical points. For example, the hcp-Ni phase has been detected in some synthesized nickel structure.[16-18] Even the non-naturally occurring bcc Ni film has been achieved by Heinrich et al.[19] and also confirmed independently by Wang et al.[20] Ferromagnetism in fcc-Ni nanowires[14,15] and hcp-Ni nanowires[18,27] is well acknowledged, respectively, but magnetic properties of bcc Ni are still under the experiment research[19-21] and theoretical calculations[22-26]. Theoretically, it is predicted by Khmelevskyi et al. that the possible existence of weak itinerant ferromagnetism in bcc Ni films prepared under compression[24]. A crucial step forward in experiment is the successful preparation of bcc Ni on GaAs (001) by C. S. Tian et al.[21], and it is proved that the bcc Ni is ferro-magnetic with a Curie temperature of 456 K. These pioneer results have opened up a unique opportunity for the investigation of the puzzling problem which is whether Ni exists meta-stable structural phase or not in nature. However, until now magnetic properties of bcc Ni are still unknown in nanowire form. To develop a deep understanding of the magnetism origin in one dimensional nanostructure, the intrinsic magnetic nature of bcc Ni is characterized in the right way unless an isolated bcc Ni phase is prepared in the laboratory. As one of the simplest and the most inexpensive methods, electro-deposition into AAO template is usually employed to prepare the nanowire arrays. In addition, an earlier experiment has indicated that a new structure phase of 4H-Ag nanowires may be obtained by electro-deposition into porous anodized aluminium oxide (AAO) templates[28].

In the present work, bcc Ni nanowires are fabricated by a multistep ac electro-deposition in anodic aluminium oxide templates, and the magnetic properties of bcc Ni nanowires are also studied. This work is not only vital to the better understanding of the self-assembling process but also significant for existence of a structure change evolving from bcc to fcc in ferromagnetic transition process. In addition, our work also establishes that fcc Ni nanowires and bulk Ni have only a ferromagnetic transition in the curie point, respectively, involving no crystal structure change.

EXPERIMENTAL PROCEDURE

A. Description of AAO template

High purity aluminium foil was used as the starting material and a two-step anodizing method was employed to obtain the AAO template[29]. After pre-treatment, the Al foil was anodized in a 0.3 mol/l $C_2H_2O_4$ solution under a dc voltage of 40 V for 2 h at 5 °C. Then the irregular alumina structure formed in the first step was stripped off by immersion into a mixture (18 g/l H_3PO_4 and 60 g/l CrO_3, 70°C) for 2 h. A second anodizing step was then carried out under the same conditions as the first step, resulting in an AAO template with a regular pore arrangement. Figure 1 shows a top view scanning electron microscopy (SEM) image of the porous AAO template prepared by this method. The average pore diameter is about 30 nm. It is clearly seen that the template including the porous AAO, barrier layer and Al substrate is shown in the inset.

B. Description of multistep ac electro-deposition method

Bcc Nickel nanowires are synthesized by a multistep ac electro-deposition method, which can be utilized to synthesize high quality and compact metal nanowires under relatively low current densities[30, 31]. Traditionally, an ac method was carried out using an ac power source with constant voltage. The constant voltage ac method requires a high current density and a high applied voltage for the tunnelling of the electrons through the barrier layer between the porous alumina layer and the Al substrate[32]. Unfortunately, a high current density makes the metal ions reduce on the inner wall of pores first and obtain many defects inside the nanowires especially resulting in nanotubes structure. On the contrary, the initial current density of the multistep ac deposition is gradually and smoothly increased step by step with increasing of the voltage, which differs from the conventional ac deposition process where the initial current density immediately increases from zero to a higher value. Within a multistep, the growth of nanowires is uniform.

Architecture AAO (amorphous)-Al film-AAO of the template is formed and works as cathode. A high-purity Platinum plate works as counter anode. Electrolyte is the mixture of 300 g/l $NiSO_4$ and 45 g/L H_3BO_3 with pH 3~4 adjusted by H_2SO_4. Electro-deposition is carried out at 9 V~16 V and a frequency of 50 Hz. After multistep ac electro-deposition, some Ni nanowire samples are heat treated at 773 K in a vacuum chamber at pressure 2.1×10^{-3} Pa for 1h. All samples are observed by TEM (JEM-2100F) and investigated by magnetic property measurement system (VSM, Lakeshore 7300). The phase structures of the samples are analyzed with the use of a Bruker D8 advanced X-ray Diffraction (XRD). The microstructures of AAO (amorphous)-Al film-AAO template are observed by SEM (JSM-7000F).

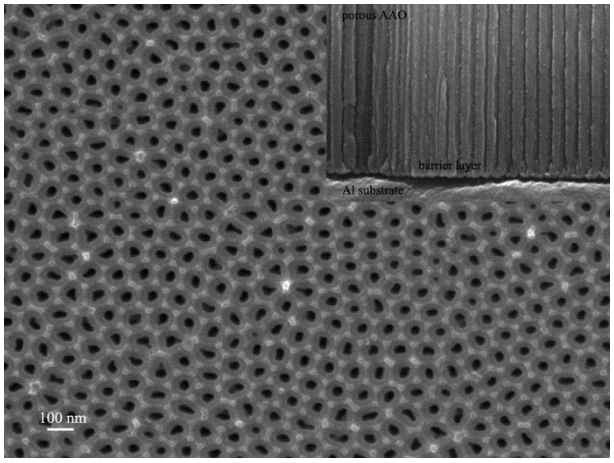

Fig.1 Top view SEM image of the porous AAO template and the inset of the cross section of the AAO template.

Results and discussion

Figure 2a shows a TEM image of Nickel nanowires after removal of the AAO template. The statistical distribution for the diameters of Nickel nanowires according to TEM characterizations in Figure 2a indicates that the Nickel nanowire has the highest concentration when the diameters are around 30 nm. Besides, the statistical data also show that the concentrations of Nickel nanowires are 6% for lower than 28 nm samples and 17% for larger than 32 nm samples, respectively. Figure 2c shows a typical TEM image of a single Nickel nanowire. It can be seen that the Nickel nanowire has a length of 1-2 μm, a diameter of 30 nm, and an aspect ratio of about 67:1, respectively. Figure 2f shows the high resolution transmission electron microscopy (HRTEM) image of the head area of Nickel nanowire, and the inset is the selected-area electron diffraction (SAED) pattern. The SAED pattern in Fig. 2f indicates that the Nickel nanowire has the single crystalline structure, and its crystal planes are in the {011} planes, and the HRTEM image in Fig. 2f indicates that the atomic arrangement *d*-spacing of the {011} crystal planes is 2.03 Å according to our measurement. As a result, it is concluded that the electron diffraction pattern of the Nickel nanowire is consistent with the characteristic picture of body-centered-cubic (bcc) in the crystal zone axis [111]. The measured spacing among these atomic rows on {011} planes are both 2.03 Å, and the lattice constant of Nickel phase is 0.288 nm according to our calculations. This is in good agreement with the previous work of Zhang et al.[33]. In Zhang's paper, bcc Ni nano-crystal was found, and the bcc Ni *d*-spacing of {011} planes was 0.206 nm.

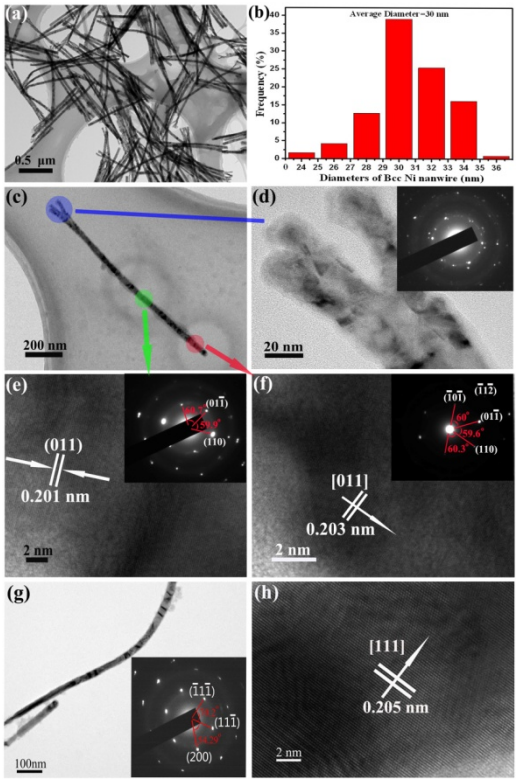

Fig.2 (a) TEM image of Ni nanowires after removal of AAO template. (b) The statistical distributions for the diameters of Ni nanowires according to TEM characterizations. (c) TEM image of a single Ni nanowire. (d) HRTEM image of the bifurcated root of Ni nanowire and its corresponding to SAED pattern (inset). (e) HRTEM image of the middle area of Ni nanowire and its corresponding to SAED pattern (inset). (f) HRTEM image of the head area of Ni nanowire and its corresponding to SAED pattern (inset). (g) TEM image of bcc Ni nanowires after heat treatment at 773 K and its corresponding SAED pattern (inset). (h) HRTEM image of the middle area of bcc Ni nanowires after heat treatment at 773 K.

It is well known that the lattice constant of face-centered-cubic (fcc) Nickel is 0.353 nm in bulk. Therefore, it is concluded that the Nickel nanowire has the single crystal bcc structure in our work. Figure 2e shows the HRTEM image of the middle area of Nickel nanowire, and the inset is the SAED pattern. The SAED pattern in Fig. 2e also shows that the Nickel nanowire has the single crystalline bcc structure, and its crystal planes are in the {011} planes. In addition, the observed and measured results in Fig. 2e are also accord with the characteristic picture of body-centered-cubic (bcc) Nickel. Figure 2d shows the HRTEM image of the bifurcated root of Nickel nanowire, and the inset is the SAED pattern, which indicates that the bifurcated root of Ni nanowire is nano-polycrystalline. The growth schematic model of the nanowires using electro-deposition method was shown by R. Sharif et al.[34] The growth process of nanowires begins from the nano-polycrystalline root, and also has been confirmed independently by Wang et al.[35]. Figure 2g shows a TEM image of the sample of bcc Ni nanowires with heat treatment at 773 K in vacuum for 1h, and the inset is the SAED pattern. In Fig. 2g, it is concluded that the electron diffraction pattern is accord with the characteristic picture of face-centered-cubic (fcc) in the crystal zone axis [011]. Figure 2h shows the HRTEM image of the middle area of the sample after heat treatment. The HRTEM image indicates that the atomic arrangement *d*-spacing of the (111) crystal plane is 2.05 Å according to our measurement, and the lattice constant of Nickel phase is 0.3551 nm according to our calculations. In other words, it can be seen that no bcc Ni phase can be found anymore, but fcc Ni phase is discovered in Fig. 2g and 2h. According to the TEM and electron diffraction pattern analysis of two structures Ni nanowires, it is concluded that bcc-Ni phase is not a stable phase, and the heat treatment can do bcc-Ni phase transit to fcc-Ni phase. In addition, a similar conclusion was also found by Tian et al.[18], for the phase transition evolving from hcp to fcc under the heating condition.

Figure 3 shows the XRD spectrum of the template of AAO (amorphous)-Al film-AAO, bcc Ni nanowire arrays in the template, respectively. In Fig.3-i, Al peaks can be identified in the spectrum due to Al originated from the template. In Fig.3-ii, extra XRD peak (211) starts to appear which can be unequivocally indexed to be from the bcc phase of Ni. Obviously, the lattice constant of bcc Ni phase as measured by XRD is 2.884 Å. Furthermore, we can identify other planes of bcc Ni according to the lattice constant of 0.2884 nm, i.e., (110) and (200), respectively. This result explains why Al peak (200) and (220) are stronger than the Al peak of the template respectively because of the overlap of the peaks coming from Ni and Al. The analysis of the XRD results indicates that the lattice constant of bcc Ni is in good line with the TEM results in experiments (shown as Fig. 2e and 2f). After heat treatment, the intensity of (211) peaks of bcc Ni disappears, and the weak peak in the 2θ range from 50° to 53° starts to appear which can be the index of (200) plane to be from the fcc phase of Ni. Obviously, the lattice constant of fcc Ni phase as measured by XRD is 3.524 Å, and we can identify other planes of fcc Ni according to the lattice constant of 0.3524 nm, i.e., (111) and (220), respectively. The analysis of the XRD results indicates that the lattice constant of fcc Ni is well consistent with the TEM results in experiments (shown as Fig. 2g and 2h).

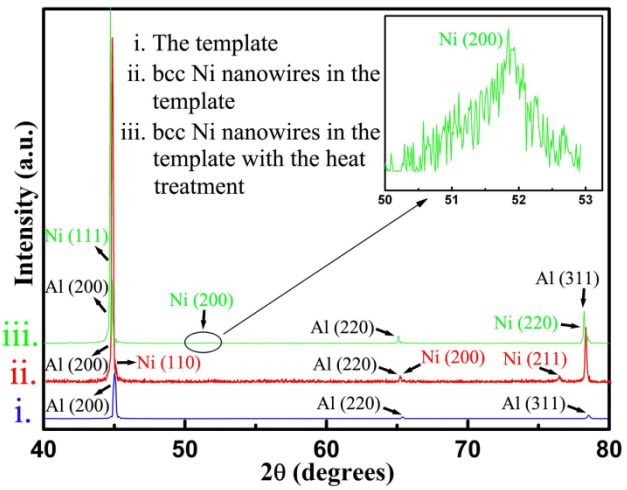

Fig.3 XRD spectrum of the template of AAO-Al film-AAO, bcc-Ni nanowire arrays in the template and bcc-Ni nanowire arrays in the template with the heat treatment at 773K, respectively.

The schematic bottom structure of AAO template is shown in Fig. 4a and 4b, in which the barrier layer could be observed clearly. Firstly, the electrons have to tunnel through the barrier layer under the driven by electric field[36], then metallic ions capture electrons and achieve the metallic-ion reduction process. Secondly, a lot of nuclei deposit in pores and achieve the growth process under the electric field. The schematic nuclei deposition process is shown in Fig. 4d. Fig. 4c shows the in situ observation of the change of voltage and current with time during the multistep electro-deposition process. During deposition, the current density ($I_{deposit}$) can be controlled by adjusting the applied voltage ($U_{deposit}$). In this work, the applied ac voltage was adjusted a little lower, in the range of 9~16 V, in order to get a relatively low current density. Firstly, when the $U_{deposit}$ increases to 9 V, the $I_{deposit}$ starts to vary with a deposition period of 16 s, and the 9 V is defined as the initial voltage ($U_{deposit\text{-}init}$); then, the deposition process is in the initial stage. The multistep rule is that the $U_{deposit}$ adds 1 V to the $U_{deposit\text{-}init}$ after the end of a previous deposition period. According to the step rule above, the $U_{deposit}$ is increased step by step to keep the deposition current density relatively stable so that the deposition process is continuous. When the $U_{deposit}$ is set higher than 16 V, the $I_{deposit}$ does not change and the deposition process is over. Clearly, the deposition under a multistep voltage only causes a low initial current density (from 16 mA to 33 mA), which is increased step by step with increasing of the voltage (from 9 V to 16 V). Such a step initial current density drives the Ni nanowires growing from the bottom to the top. This growth process is favourable to form a uniform microstructure.

Based on our experimental results, the size effect in bcc-Ni nanowires can be interpreted through nano-pore limited growth in the AAO templates. Nickel is well-known as a FCC metal in its bulk form because FCC-Ni has a lower internal energy when surface and interface effect can be neglected. However, the diameter of bcc Ni nanowire is only several tens of nanometers, the size effect should be taken into account. The sized-parameters (e.g., the internal energy) provide a strong and clear signature of

structural changes in nanowire[37]. Furthermore, a strong size effect was realized for the 4H structural silver nanowire (4H-AgNW), which is attributed to a higher volume internal energy than FCC-AgNW[28]. Therefore, the dependence of γ (crystal-melt interfacial free energy) on crystal structure is crucial to understanding the role of meta-stable structure in nucleation pathways[38]. In 1897, Ostwald[39] formulated his "step rule," which states that nucleation from the melt occurs to the phase with the lowest activation barrier, which is not necessarily the thermodynamically most stable bulk phase. Davidchack et al indicated[38] that in the case of the nucleation of face-centered-cubic (fcc) crystals, there is evidence that crystallization often proceeds first through the formation of body-centered-cubic (bcc) nuclei, which transform to fcc crystallites later in the growth process. This phenomenon has been observed in computer simulations of Lennard-Jones particles[40] and weakly charged colloids[41].

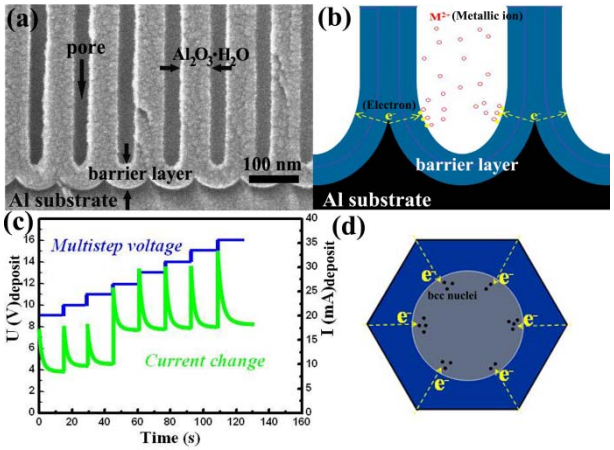

Fig.4 Barrier structure of AAO template. (a) Cross section view SEM image of AAO template and (b) Schematic diagrams for electrodepositing metallic ions upon barrier layer. (c) In situ observation of the change of voltage and current with time during the multistep electro-deposition process. (d) The schematic nuclei deposition process.

The magnetic properties of bcc Ni nanowires within the AAO template are studied by VSM with various θ, which is the angle between the applied magnetic field and the axial direction of bcc Ni nanowires. Figure 5a shows the magnetization (M) depending on the applied magnetic field (H) M-H loops of bcc Ni nanowires. When the external magnetic field is parallel to the axial direction of bcc Ni nanowires (θ=0°), $H_{c//}$ is about 734 Oe. When the external magnetic field is perpendicular to the axial direction of bcc Ni nanowires (θ=90°), the $H_{c\perp}$ is about 193 Oe, which is much smaller than $H_{c//}$ of θ=0° . Moreover, it can be seen that the squareness S (S= M_r/M_s where M_r denotes remanence and M_s denotes the saturation magnetization) in the parallel direction is higher than that in the perpendicular direction, that is $S_{//}$=0.97 at θ=0° , $S_{\perp}$=0.11 at θ=90° . Therefore, it can be proved that bcc Ni is ferromagnetic phase, and bcc Ni nanowires exhibit a typical magnetic anisotropy, which is dominantly attributed to the shape anisotropy due to the aspect ratio of about 67:1. The change curves of H_c and M_r/M_s as a function of θ are shown in Fig. 5b. Both the H_c and the M_r/M_s decrease with an increase in θ, which means that bcc Ni nanowires behave with obvious magnetic anisotropy and with the easy axis along bcc Ni nanowires.

Some theories have been established to explain the magnetic reversal mechanism of magnetic nanowires[42-44]. The chain-of-spheres model[42] was considered to be the most useful according to previous reports[45-48]. Basing on the chain-of-spheres model, the nanowire can be viewed as a chain of single-domain magnetic spheres; there is no shape anisotropy. Also, the spheres are assumed to make point contact or even to be slightly separated resulting in magnetic isolation.

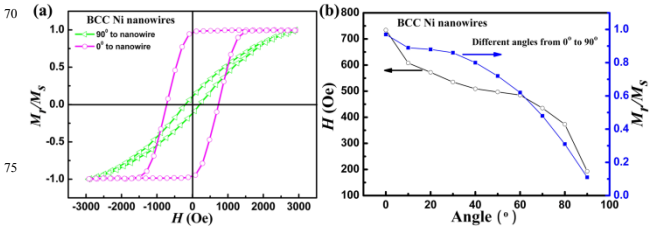

Fig.5 (a) M-H loops of the bcc Ni nanowires when θ=0° and θ=90° (where θ is the angle between the applied magnetic field and the axial direction of the nanowires). (b) Change curves of coercivity H_c and remnant ratio M_r/M_s of bcc Ni nanowires depending on different θ.

In our previous work[30], we proved that the calculated H_c from the chain of prolate spheroids model agrees well with the experiment result by the multistep method for the Co nanowires. Figure 6b shows the HRTEM image of bcc Ni nanowire, which the prolate spheroid particles can be viewed as a chain of prolate spheroids structure, as shown in Fig. 6a. The H_c of bcc Ni nanowires should be

$$H_{c,n} = (\mu/a^3)(6K_n - 4L_n) + (N_t - N_o)I_s, \quad (1)$$

where the coercivity ($H_{c,n}$) is divided to the following two parts: $(\mu/a^3)(6K_n - 4L_n)$ is the contribution from the magnetic inter-action, and $(N_t - N_o)I_s$ is contributed from the shape anisotropy[42], where n is the number of spheroids, ($H_{c,n}$) is the coercivity of the chain with n prolate spheroids, a is the distance between the centers of adjacent spheroids, μ is the dipole moment of one spheroid, N_o and N_t are the shape demagnetization factors of a prolate spheroid along the major and minor axes, and I_s is the saturation magnetization of bcc Ni. K_n and L_n are given as

$$L_n = \sum_{j=1}^{\frac{1}{2}(n-1)<j\le\frac{1}{2}(n+1)} \left[n - (2j-1) / n(2j-1)^3 \right], \quad (2)$$

$$M_n = \sum_{j=1}^{\frac{1}{2}(n-2)<j\le\frac{1}{2}n} \left[(n-2j) / n(2j)^3 \right], \quad (3)$$

$$K_n = L_n + M_n, \quad (4)$$

where j is an integer from 1 to n.

For the bcc Ni nanowires in this paper, the magnetic moment is (0.52 ± 0.08) μ_B/atom[21]; thus, the I_s is equal to 0.507×10^6 (A/m).

Here, the number of n in the model is 12 due to the scale of the model restricted by heavy computation cost. As a result, the $H_{c,n}$ calculated from Eq. (1) is about 780 Oe. Therefore, although there is a small difference between the calculated value and the experimental result, the chain of prolate spheroids model is more consistent with the bcc Ni nanowires produced in this work.

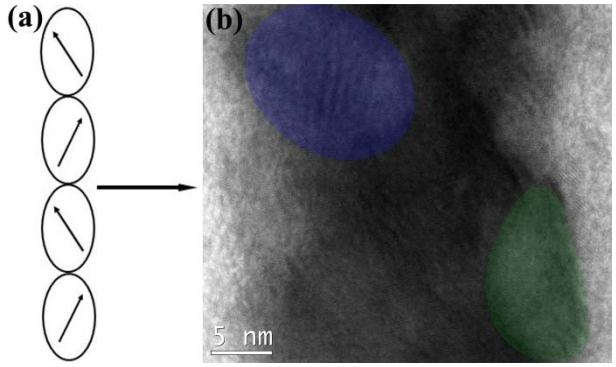

Fig.6 (a) Chain-of-prolate-spheroids model. (b) TEM image of the prolate spheroid particles in the bcc Ni nanowire (Color).

In order to study magnetic state and the nature of the magnetism, bcc Ni nanowires are studied in the temperature range of 300 K ~ 773 K by temperature-dependent zero-field-cooled (*ZFC*) and field-cooled (*FC*) magnetization measurements in a low external magnetic field (H=200 Oe). Figure 7c shows the temperature-dependent *ZFC* and *FC* magnetization of bcc Ni nanowires measure under applied field of 200 Oe. *ZFC* curve shows the magnetization decreases gradually, with slow increase of the temperature, and increases steeply when the heat temperature is higher than 550 K, followed by a sharp drop in magnetization at the ferromagnetic transition temperature. At the lower temperature, *FC* curve does not retrace the *ZFC* curve at a magnetization value corresponding to the demagnetizing limit of the sample. This phenomenon is very different from *ZFC* curve and *FC* curve of bulk fcc-Ni, as shown in Fig. 7f. *ZFC* curve of bulk fcc-Ni shows that the magnetization increases gradually along with the temperature rising, and when the temperature reaches to 631 K (T_c) fcc-Ni bulk material takes place ferromagnetic transition, which involves no structure change. The situ heating TEM images of bcc Ni nanowires are shown in Fig. 7a, 7b and 7d. Before heating, bcc Ni structure in the nanowire is confirmed in Fig. 7a (1, 2). Up to 646 K for 5 min, no change in the as deposited bcc Ni structure is observed in Fig. 7b (1, 2). All electron diffraction spots can be identified as a bcc phase. Above 773 K for 40 min, the twin structure of the nanowire starts to appear in Fig. 7d (1, 2). Figure 7d (2) indicates that the electron diffraction pattern of the nanowire is the characteristics of twin diffraction pattern which can be the index of (111) twin plane to be from the fcc phase of Ni. As the result, it is concluded that the structure transition evolving from bcc to fcc is proved by in situ heating in the TEM, and this result is accord with the variation behaviour of the magnetization in *ZFC* curves (Fig. 7c). Figure 7e is *ZFC* and *FC* curve of the sample of bcc Ni nanowires with heat treatment at 773 K. From Fig. 7e, the *ZFC* curve shows that the magnetization increases gradually along with the temperature rising, and the variation behaviour of the magnetization is similar to *ZFC* curve of bulk Ni (Fig. 7f). The temperature-dependent *ZFC* and *FC* curves of three types of Ni materials (bcc nanowires, fcc nanowires and bulk) indicate that the magnetization process of bcc-Ni phase is very different from the process of fcc-Ni phase, and involves structure transition evolving from bcc to fcc at T_S =450 K (where the superscript S represents the structure transition). In addition, similar conclusion was also found by C. S. Tian et al. that the Curie temperature of bcc Ni film is 456 K[21].

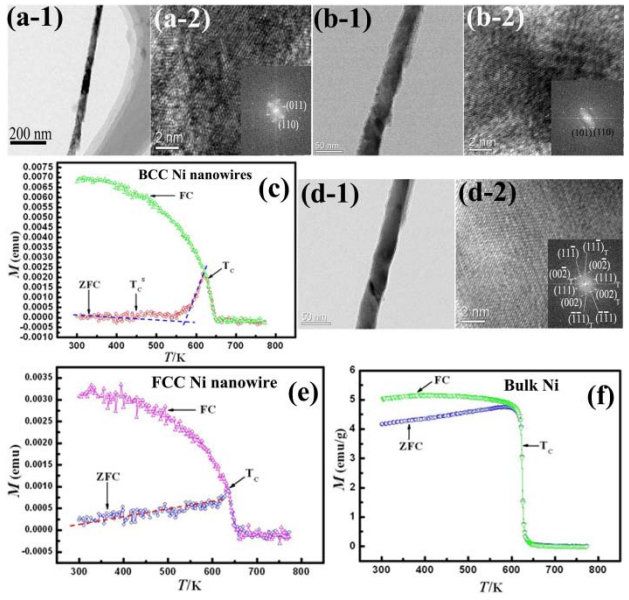

Fig.7 In situ TEM diffraction series at different temperatures from RT to 773K, including TEM image of single nanowire, HRTEM image of the middle area and its corresponding selected-area FFT image (inset), respectively. (a) Bcc Ni nanowire at room temperature; (b) Bcc Ni nanowire with heat treatment at 646K; (d) bcc Ni nanowire with heat treatment at 773K. The dependence of *ZFC* and *FC* on temperature curves. (c) Bcc Ni nanowires; (e) The sample of bcc Ni nanowires with heat treatment at 773 K; (f) Bulk Ni.

As demonstrated above, the thermal field can induce bcc-Ni phase transit to fcc-Ni phase. On the other hand, it was also found by Zhang et al.[33] that the strain field can induce the fcc-to-bcc phase transformation in nano-crystalline nickel. Figure 8a shows the schematic of the structure change from body-centered-cubic to face-centered-cubic. To obtain results for the body-centered-tetragonal lattice, a bcc lattice is subjected to W uniaxial deformation along one of the edges of the unit cell. Furthermore, the lattice c of the uniaxial deformation is equal to κa, where the ratio c/a is to κ. Lastly, the bct unit cell along W uniaxial contra rotating 45° forms two unit cells of the fcc crystal, which the relationship between the bct and fcc unit cells is meted for bct with c/a equal to $\sqrt{2}$. It is well known that the allotropic transformation of Fe metal involves structure variation from bcc to fcc at 1185 K, and the Curie temperature T_c of Fe is 1043 K. The research of the thermodynamics of phase transformation for Fe metal was reported by Nishizawa[49] shown in Fig. 8 (b, c). It

can be seen that A_3 presents the structural change from fcc to bcc at 1185 K, and A_2 indicates the magnetic transition of Fe at 1043 K. Moreover, Nishizawa also suggested[49] that the magnetic transition of Fe was the reason that the abnormal transition (structure transition from fcc to bcc) occurred at 1185 K, and the magnetic transition of Fe was a first order phase transition.

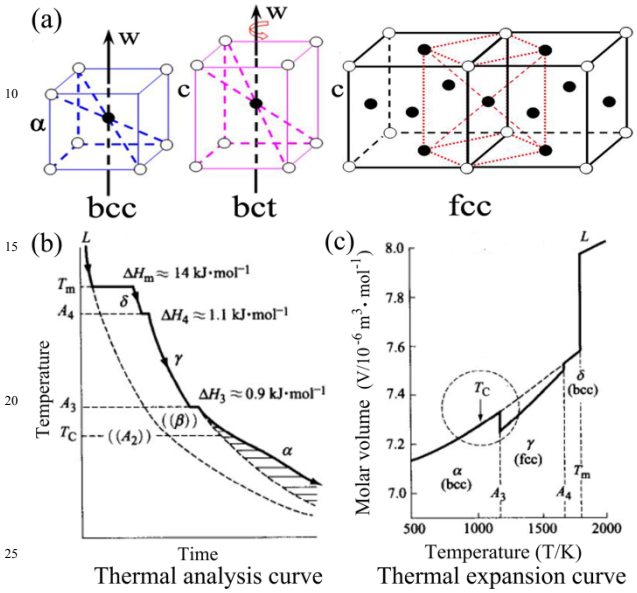

Fig.8 (a) The schematic of the structure change from body-centered-cubic to face-centered-cubic. (b) The thermal analysis curve of Fe (Ref. 49). (c) The thermal expansion curve of Fe (Ref. 49).

Conventional diffractometry over the past decades has revealed that the ferromagnetic transition, an ordering of the magnetic moment, involves no crystal structure change in general, thus a cubic paramagnet has been considered to transform into a cubic ferro-magnet upon a ferromagnetic transition. However, the simultaneous structural change at the ferromagnetic transition was found by Yang et al.[50,51], for the structure change of $CoFe_2O_4$, Terfenol-D, and $DyCo_2$ in situ higher-solution synchrotron x-ray diffractometry (XRD) observation. Moreover, Yang also proved[50,51] in experimental and theoretically that ferromagnetic transition is a structural transition, yielding a low crystallographic symmetry that conforms to the spontaneous magnetization (M_S) direction. Therefore, our work has proved experimentally that the ferromagnetic transition of bcc Ni nanowires involves a structure change evolving from bcc to fcc in magnetic-ordering process. This seems to support the experimental results by Nishizawa and Yang[49-51]. This interesting point is waiting for a future study.

Conclusions

In summary, we have achieved for the first time magnetically isolated single-crystalline bcc Nickel nanowires by a multistep ac electro-deposition in anodic aluminium oxide templates. BCC Ni is ferromagnetic with a lattice constant of 0.288 nm, and bcc-Ni to fcc-Ni phase transition occurs in heat treatment. We show that the ferromagnetic transition of bcc Ni nanowires is not just an ordering of the magnetic moment alone; it also involves a structure change evolving from bcc to fcc. Finally the processes of structure transition in bcc Ni nanowires under the heating conditions are observed in situ by transmission electron microscopy.

Acknowledgments

This work is financially supported by the National Natural Science Foundation of China (Grant No. 51371134). The authors are grateful to Dr. Wen Guan for VSM measurement and Dr. Yu Wang for helpful discussion.

Notes and references

[a]*MOE Key Laboratory for Nonequilibrium Synthesis and Modulation of Condensed Matter& State Key Laboratory for Mechanical Behaviour of Materials, School of Science, Xi'an Jiaotong University, Xi'an 710049, People's Republic of China. E-mail: han.ch@stu.xjtu.edu.cn and xpsong@mail.xjtu.edu.cn.*
[b]*Department of Mechanical Engineering, University of Tokushima, Tokushima 7708506, Japan. E-mail: wangpp@mail.xjtu.edu.cn.*

† Electronic Supplementary Information (ESI) available: [details of any supplementary information available should be included here]. See DOI: 10.1039/b000000x/

1 Florian Maurer, Joachim Brötz, Shafqat Karim, Maria Eugenia Toimil Molares, Christina Trautmann and Hartmut Fuess, *Nanotechnology.*, 2007, **18**, 135709.
2 Bhabendra K. Pradhan, Takashi Kyotani and Akira Tomita, *Chem. Commun.*, 1999, 1317.
3 Tzong-Jer Yang, Yu-Jun Zhao, A. J. Freeman, *J. Magn. Magn. Mater.*, 2004, **272-276**, 1648.
4 E. J. Menke, M. A. Thompson, C. Xiang, L. C. Yang, and R. M. Penner, *Nature Mater.*, 2006, **5**, 914-916.
5 Bongyoung Yoo, Youngwoo Rheem, Ward P Beyermann and Nosang V Myung, *Nanotechnology.*, 2006, **17**, 2512-2517.
6 T. Koyama, D. Chiba, K. Ueda, K. Kondou, H. Tanigawa, S. Fukami, T. Suzuki, N. Ohshima, N. Ishiwata, Y. Nakatani, K. Kobayashi and T. Ono, *Nature Mater.*, 2011, **10**, 194-197.
7 Bozhi Tian, Jia Liu, Tal Dvir, Lihua Jin, Jonathan H. Tsui, Quan Qing, Zhigang Suo, Robert Langer, Daniel S. Kohaneand CharlesM. Lieber, *Nature Mater.*, 2012, **11**, 986-994.
8 Joseph Wang, Mustafa Musameh, Rawiwan Laocharoensuk, *Electrochem Commun.*, 2005, **7**, 652-656.
9 Seema Prasad, N. S. Gajbhiye, *J Alloy Compd.*, 1998, **265**, 87-92.
10 A. Kale, S. Gubbala, R. D. K. Misra, *J. Magn. Magn. Mater.*, 2004, **277**, 350-358.
11 D. -X. Chen, O. Pascu, A. Roig, A. Sanchez, *J. Magn. Magn. Mater.*, 2010, **322**, 3834-3840.
12 Shiro Entani, Mitsunori Kurahashi, Xia Sun, Yasushi Yamauchi, *Carbon.*, 2013, **61**, 134-139.
13 K. J. Veenstra, P. E. Hansen, A. Kirilyuk, A.V. Petukhov, Th. Rasing, *J. Magn. Magn. Mater.*, 1999, **198-199**, 695-697.
14 Mousa M.A. Imran, J. *Alloys Compd.,* 2008, **455**, 17-20.
15 A. L. Dolgiy, S. V. Redko, I. Komissarov, V.P. Bondarenko, K.I. Yanushkevich, S.L. Prischepa, *Thin Solid Films.*, 2013, **543**, 133-137.
16 Mireille Richard-Plouet, Murielle Guillot, Serge Vilminot, Cédric Leuvrey, Claude Estournès, and Mohamedally Kurmoo, *Chem. Mater.*, 2007, **19**, 865-871.
17 Abhishek Lahiri, Rupak Das, Ramana G. Reddy, *J. Power. Sources*, 2010, **195**, 1688-1690.
18 F. Tian, J. Zhu, and D. Wei, *J. Phys. Chem. C*, 2007, **111**, 6994-6997.
19 B. Heinrich, A. S. Arrotf, J. F. Cochran, S.T. Purcell, K.B. Urquhart, K. Myrtle, *J Cryst Growth.*, 1987, **81**, 562-569.
20 Z. Q. Wang, Y. S. Li, F. Jona, *Solid State Commun.*, 1987, **61**, 623-626.
21 C. S. Tian, D. Qian, D. Wu, R. H. He, Y. Z. Wu, W. X. Tang, L. F. Yin, Y. S. Shi, G. S. Dong, and X. F. Jin, *Phys. Rev. Lett.*, 2005, **94**, 137210.
22 V. L. Moruzzi, *Phys. Rev. Lett.*, 1986, **57**, 2211-2214.

23 V. L. Moruzzi and P. M. Marcus, *Phys. Rev. B.*, 1986, **34**, 1784-1791.
24 S. Khmelevskyi, P. Mohn, *Phys. Rev. B.*, 2007, **75**, 012411.
25 C. Etz, A. Vernes, L. Szunyogh, P. Weinberger, *Phys. Rev. B.*, 2008, **77**, 064420.
26 M. Zeleny, D. Legut, M. Sob, *Phys. Rev. B.*, 2008, **78**, 224105.
27 Zhida Cheng, Jing Zhu, and Zheng Tang, *J. Appl. Phys.*, 2009, **105**, 103906.
28 Xiaohua Liu, Jun Luo, Jing Zhu, *Nano Lett.*, 2006, **6**, 408-412.
29 H. Masuda and K. Fukuda, *Science*, 1995, **268**, 1466.
30 Pangpang Wang, Lumei Gao, Zhiyong Qiu, Xiaoping Song, Liqun Wang, Sen Yang, and Ri-ichi Murakami, *J. Appl. Phys.*, 2008, **104**, 064304.
31 Chang Huang, Pangpang Wang, Wen Guan, Sen Yang, Lumei Gao, Liqun Wang, Xiaoping Song , Ri-ichi Murakami, *Materials Letters*, 2010, **64**, 2465-2467.
32 F. Keller, M S. Hunter and D.L. Robinson, *Journal of The Electrochemical Society*, 1953, **100**, 411.
33 X. Y. Zhang, X. L. Wu, Q. Liu, R. L. Zuo, A. W. Zhu, P. Jiang, and Q. M. Wei, *Appl. Phys. Lett.*, 2008, **93**, 031901.
34 R. Sharif, S. Shamaila, M. Ma, L.D. Yao, R.C. Yu, X.F. Han, Yong Wang, M. Khaleeq-ur-Rahman, *J. Magn. Magn. Mater.*, 2008, **320**, 1512.
35 Biao Wang, Guang Tao Fei, Ye Zhou, Bing Wu, Xiaoguang Zhu, and Lide Zhang, *Cryst. Growth Des.*, 2008, **8**, 3073.
36 Kornelius Nielsch, Frank Müller, An-Ping Li, and Ulrich Gösele, *Adv. Mater.*, 2000, **12**, 582.
37 Ruslan L. Li Hui, F. Pederiva, B. L. Wang, J. L. Wang, and G. H. Wang, *Appl. Phys. Lett.*, 2005, **86**, 011913.
38 Ruslan L. Davidchack, *Phys.Rev.Lett.*, 2005, **94**, 086102.
39 W. Ostwald, *Z. Phys. Chem.*, 1897, **22**, 289.
40 Pieter Rein ten Wolde et al., *Phys. Rev. Lett.*, 1995, **75**, 2714.
41 S. Auer, D. Frenkel, *J. Phys. Condens. Matter.*, 2002, **14**, 7667.
42 I. S. Jacobs and C. P. Bean, *Phys. Rev.*, 1955, **100**, 1060.
43 E. H. Frei, S. Shtrikman, and D. Treves, *Phys. Rev.*, 1957, **106**, 446.
44 X. Lu, S. Ge, L. Jiang, and X. Wang, *J. Appl. Phys.*, 2005, **97**, 084304.
45 T. M. Whitney, J. S. Jiang, P. C. Searson, and C. L. Chien, *Science*, 1993, **261**, 1316.
46 G. Kartopu, O. Yalçın, M. Es-Souni, and A. C. Başaran, *J. Appl. Phys.*, 2008, **103**, 093915.
47 P. S. Fodor, G. M. Tsoi, and L. E. Wenger, *J. Appl. Phys.*, 2002, **91**, 8186.
48 J. Zhang, G. A. Jones, T. H. Shen, S. E. Donnelly, and G. Li, *J. Appl. Phys.*, 2007, **101**, 054310.
49 Taiji Nishizawa, *Thermodynamics of Microstructures*, 2008, 40-45.
50 Sen Yang, Xiaobing Ren, *Phys. Rev. B.*, 2008, **77**, 014407.
51 Sen Yang, Huixin Bao, Chao Zhou et al., *Phys. Rev. Lett.*, 2010, **104**, 197201.

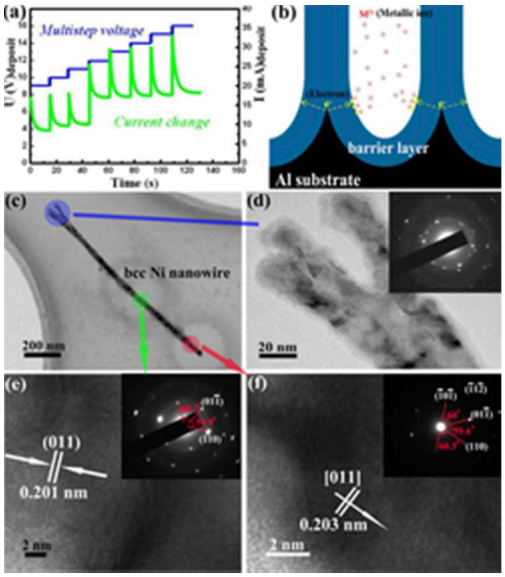

Body-Centered-Cubic (BCC) Ni nanowires have been successfully synthesized by a multistep ac electro-deposition in anodic aluminium oxide templates.
10x11mm (600 x 600 DPI)